Eulerian framework for bubble-cloud–kidney stone interaction

Jean-Sebastien Spratt*, Mauro Rodriguez, Spencer H. Bryngelson, Shunxiang Cao, Tim Colonius

Division of Engineering and Applied Science, California Institute of Technology, Pasadena, CA 91125, USA

Abstract

Burst-wave lithotripsy (BWL) is a therapy for ablating kidney and gall bladder stones. During therapy, high-amplitude ultrasound waves issue from a transducer array and focus near the stone. These waves can nucleate clouds of small bubbles at the surface of the stone. This can affect treatment efficacy: acoustic shielding due to the bubble clouds can attenuate stone breakup, though the collapse of individual bubbles can amplify it. Further, these collapses can cause damage to surrounding tissue. Thus, optimizing lithotripsy against potential damage requires predicting bubble-stone interactions. Simulating bubble cloud cavitation is challenging due to the breadth of spatio-temporal scales involved. Additional scale restrictions are associated with soft material dynamics, which interact with the bubble clouds during lithotripsy. The open-source solver MFC can address these challenges [1]. It uses a phase-averaging sub-grid model for bubble cloud cavitation and has been extended to include a hypoelastic Kelvin–Voigt model to compute stresses in stones and nearby soft surfaces. These models are fully-coupled to the fluid dynamics. The capabilities of this approach are demonstrated for a model BWL problem. The stress state in a kidney stone is modeled during treatment.

Keywords: soft matter, hypoelasticity, bubble dynamics, lithotripsy

1. Introduction

Burst-wave lithotripsy (BWL) has recently been developed as an alternative to shock-wave lithotripsy (SWL) for the treatment of kidney stones. Both therapies use multiple rounds of focused waves to ablate stones, enabling patients to pass them naturally once small enough [2]. While SWL has been shown to be an effective treatment, there is evidence that it can, in some cases, cause significant injury to patients [3, 4]. Hence, BWL, which uses smaller amplitude bursts of focused ultrasound, has proved to be a compelling alternative with less potential for damage. Experiments [5, 6] have demonstrated the treatment's efficacy for kidney stone breakdown. Furthermore, BWL tends to produce internal cracks within the entire stone that leads to small fragments whose size can be regulated by the ultrasound frequency [7, 5].

To optimize treatment efficacy and minimize potential damage to surrounding tissues across, we develop a framework for high fidelity simulations of BWL. Such simulations could predict BWL efficacy in a wide array of cases, with varying transducer configurations, stone composition and geometries. Furthermore, during treatment, cavitating bubble clouds can nucleate near the stone and affect treatment [8]. These bubble clouds directly can either attenuate the breakup through acoustic shielding, or enhancing it through violent collapse of individual bubbles. Thus, to fully model BWL and understand these effects, simulations should incorporate bubble clouds and an accurate stone model. In this paper, we demonstrate MFC's ability to simulate BWL and similar

*Corresponding author; jspratt@caltech.edu

phenomena, using phase-averaging sub-grid bubble model and a hypoelastic material model for the stone. In section 2, MFC and the added hypoelastic material model are presented. In section 3, results of validation and sample simulations are discussed.

2. Materials and Methods

2.1. Multi-component Flow Code (MFC) solver

MFC is an open-source high-order-accurate multi-component flow solver. It uses interface-capturing, HLL-type approximate Riemann solvers, and total-variation-diminishing time-integration schemes to solve for a wide range of flows [1]. In particular, the 5-equation diffuse-interface model is used to represent compressible multi-component flows [9]. MFC models bubbly flows via a sub-grid ensemble-phase-averaged model [10], which has already been verified [11] and used in various studies [12]

2.2. Hypoelasticity Implementation

We use a hypoelastic constitutive model to represent the solid mechanics of BWL in an Eulerian framework. This model, suitable for small strains [13], uses an objective temporal derivative of the constitutive relation to avoid calculating strains [14]. Instead, strain rates are obtained from velocity gradients. An elastic shear stress $\tau_{ij}^{(e)}$ contributes to the Cauchy stress tensor as

$$\sigma_{ij} = -p\delta_{ij} + \tau_{ij}^{(v)} + \tau_{ij}^{(e)}, \tag{1}$$

where p is the pressure and $\tau_{ij}^{(v)}$ the viscous shear stress contribution. Then, modeling materials as Neo-Hookean Kelvin–Voigt media, we can write $\dot{\tau}_{ij}^{(e)} = 2G\dot{\epsilon}_{ij}^{(d)}$, where $\dot{\epsilon}_{ij}^{(d)}$ is the deviatoric shear strain rate tensor and the Lie objective temporal derivative [15] is used to solve the equation. Adding the elastic stress contributions and this evolution equation to the usual 5-equation model [16] yields, for 2 materials,

$$\frac{\partial}{\partial t}\begin{bmatrix} \alpha^{(1)} \\ \alpha^{(1)}\rho^{(1)} \\ \alpha^{(2)}\rho^{(2)} \\ \rho u_i \\ \rho E \\ \rho\tau_{il}^{e} \end{bmatrix} + \frac{\partial}{\partial x_j}\begin{bmatrix} \alpha^{(1)}u_j \\ \alpha^{(1)}\rho^{(1)}u_j \\ \alpha^{(2)}\rho^{(2)}u_j \\ \rho u_i u_j + p\delta_{ij} - \tau_{ij}^{v} - \tau_{ij}^{e} \\ (\rho E + p - \tau_{ij}^{e})u_j - u_i\tau_{ij}^{v} \\ \rho\tau_{il}^{e}u_j \end{bmatrix} + \begin{bmatrix} -\alpha^{(1)} - K \\ 0 \\ 0 \\ 0 \\ 0 \\ 0 \end{bmatrix} \frac{\partial u_j}{\partial x_j} = \begin{bmatrix} 0 \\ 0 \\ 0 \\ 0 \\ 0 \\ S_{il}^{e} \end{bmatrix}, \tag{2}$$

where superscripts (1) and (2) are indices corresponding to different materials, $\alpha^{(k)}$ is the k-th volume fraction, u_j the velocity in the j-th direction, E the total energy, and K the interface compressibility term. The right-hand-side terms to the elastic shear stress evolution equation are

$$S_{il}^{e} = \rho\left(\tau_{kj}^{(e)}\frac{\partial u_i}{\partial x_k} + \tau_{ik}^{(e)}\frac{\partial u_j}{\partial x_k} - \tau_{ij}^{(e)}\frac{\partial u_k}{\partial x_k} + 2G\dot{\epsilon}_{ij}^{(d)}\right). \tag{3}$$

An elastic contribution $e^{(e)} = \frac{\tau_{ij}^{(e)}\tau_{ij}^{(e)}}{4\rho G}$ is added to the total energy, yielding $E = e + \|\boldsymbol{u}\|^2/2 + e^{(e)}$, where e is the internal energy. Finally, the system is closed using the stiffened-gas equation of state

$$p_k = (\gamma_k - 1)\rho)ke_k - \gamma_k\pi_{\infty,k}. \tag{4}$$

3. Results

3.1. Validation

We validate our implementation of material hypoelasticity via two test cases. The first is a one-dimensional shock tube considered by Gavrilyuk et al. [17] and Rodriguez and Johnsen [14] with a $1000:1$ pressure jump and y-velocity discontinuity in an elastic material. Its initial conditions are

$$(\rho, u, v, p, \tau_e, G) = \begin{cases} (10^3, 0, \quad 100, 10^8, 0, 10^{10}) & \text{for } x \in [0, 0.5), \\ (10^3, 0, -100, 10^5, 0, 10^{10}) & \text{for } x \in [0.5, 1]. \end{cases}$$

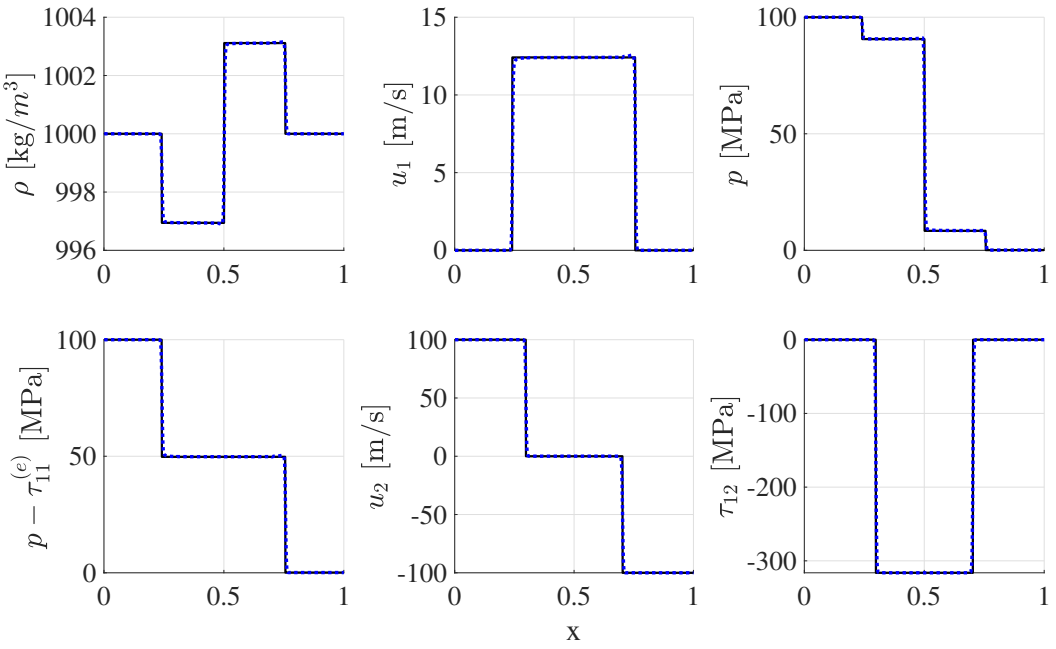

Figure 1: Comparing the MFC solution (blue dotted line) to the exact solution (black line) for a 1D shock tube problem at $t = 64\,\mu\text{s}$

Results are shown in figure 1. Five waves are observed: a shock propagating to the right, a rarefaction propagating to the left, a contact discontinuity in the center, and shear waves propagating in both directions. Simulation results show good agreement with the exact solution, notably demonstrating correct p-wave and s-wave speeds in this elastic material.

Next, we consider a two-dimensional simulation of bi-layered media to examine transmitted s- and p-waves through a water–elastic-medium interface. An acoustic source in the top fluid layer, 500 m above the interface, generates one cycle of a 10 Hz Ricker wave. The elastic material has density $\rho = 2500\,\text{kg/m}^3$ and theoretical wave-speeds $c_p = 3400\,\text{m/s}$ and $c_s = 1963\,\text{m/s}$.

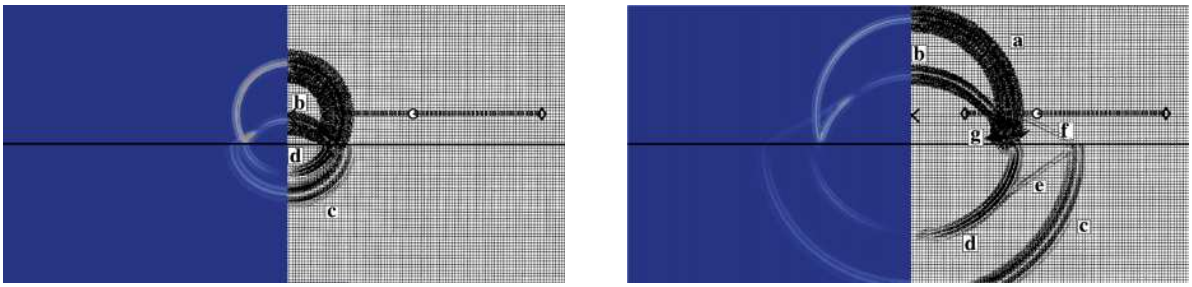

(a) $t = 0.7\,\mathrm{s}$ **(b)** $t = 1.26\,\mathrm{s}$

Figure 2: Comparison of present velocity magnitude (left half-space) with the velocity vectors (right half-space) associated with the spectral element code of Komatitsch et al. [18] at two different times t as labeled.

Figure 2 compares results of the present implementation with the spectral-element-method based simulation of Komatitsch et al. [18]. The simulation displays all expected waves: a (b) reflected and (c) transmitted p-wave, a (d) transmitted s-wave, and (e,f) refracted waves. Calculated p and s-wave speeds in the elastic medium match the values expected from theory within 0.1%.

3.2. BWL simulation

We next simulate BWL via a two-dimensional domain and a hypoelastic model stone. A transducer array focuses 10 pulses of 370 kHz ultrasound with an amplitude of 6.5 MPa onto a stone characterized by $\rho = 2040\,\mathrm{kg/m^3}$, $c_p = 3640\,\mathrm{m/s}$, and $c_s = 2035\,\mathrm{m/s}$. These values correspond to the density and wave-speeds of an artificial kidney stone (called Begostone), and fall within the range of values seen in human urinary stones [7]. The stone is submerged in water.

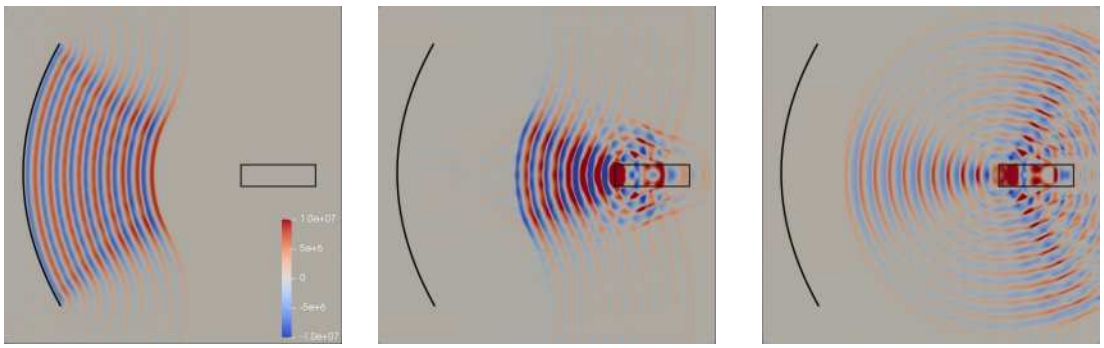

(a) $t = 25\,\mu\mathrm{s}$ **(b)** $t = 50\,\mu\mathrm{s}$ **(c)** $t = 70\,\mu\mathrm{s}$

Figure 3: Pressure in the liquid and maximum principal stress in the stone at three different times during MFC simulation of BWL

Figure 3 shows the pressure in the liquid, and maximum principal stress in the stone in the absence of any cavitating bubbles. Ultrasound waves emitted by the transducer focus on the model stone, and create high stress concentrations which propagate through the stone. While a direct comparison cannot be made, the stress pattern observed in the stone resembles those observed at the same frequency experimentally by Maxwell et al. [7] via photoelastic imaging. Such simulations can be run for various test cases, varying stone geometry and composition, transducer frequency and focal point, and so on. Hereby, MFC can serve as a powerful tool to optimize BWL administration.

4. Acknowledgments

This work was supported by the National Institutes of Health under grant number 2P01-DK043881 and the US Office of Naval Research under grant numbers N0014-17-1-2676 and N0014-18-1-2625.

References

[1] S. H. Bryngelson, K. Schmidmayer, V. Coralic, J. C. Meng, K. Maeda, T. Colonius, MFC: An open-source high-order multi-component, multi-phase, and multi-scale compressible flow solver, Computer Physics Communications (2020) 107396.

[2] J. Jendeberg, H. Geijer, M. Alshamari, B. Cierzniak, M. Lidén, Size matters: The width and location of a ureteral stone accurately predict the chance of spontaneous passage, European Radiology 27 (2017) 4775–4785.

[3] J. A. McAteer, A. P. Evan, The acute and long-term adverse effects of shock wave lithotripsy, Seminars in Nephrology 28 (2008) 200–213.

[4] M. R. Bailey, Y. A. Pishchalnikov, O. A. Sapozhnikov, R. O. Cleveland, J. A. McAteer, N. A. Miller, I. V. Pishchalnikova, B. A. Connors, L. A. Crum, A. P. Evan, Cavitation detection during shock-wave lithotripsy, Ultrasound in Medicine & Biology 31 (2005) 1245–1256.

[5] A. D. Maxwell, B. W. Cunitz, W. Kreider, O. A. Sapozhnikov, R. S. Hsi, J. D. Harper, M. R. Bailey, M. D. Sorensen, Fragmentation of urinary calculi in vitro by burst wave lithotripsy, Journal of Urology 193 (2015) 338–344.

[6] J. D. Harper, I. Metzler, M. K. Hall, T. T. Chen, A. D. Maxwell, B. W. Cunitz, B. Dunmire, J. Thiel, J. C. Williams, M. R. Bailey, M. D. Sorensen, First in-human burst wave lithotripsy for kidney stone comminution: Initial two case studies, Journal of Endourology (2020).

[7] A. D. Maxwell, B. MacConaghy, M. R. Bailey, O. A. Sapozhnikov, An investigation of elastic waves producing stone fracture in burst wave lithotripsy, The Journal of the Acoustical Society of America 147 (2020) 1607–1622.

[8] K. Maeda, A. D. Maxwell, T. Colonius, W. Kreider, M. R. Bailey, Energy shielding by cavitation bubble clouds in burst wave lithotripsy, The Journal of the Acoustical Society of America 144 (2018) 2952–2961.

[9] G. Allaire, S. Clerc, S. Kokh, A five-equation model for the simulation of interfaces between compressible fluids, Journal of Computational Physics 181 (2002) 577–616.

[10] D. Z. Zhang, A. Prosperetti, Ensemble phase-averaged equations for bubbly flows, Physics of Fluids 6 (1994) 2956–2970.

[11] S. H. Bryngelson, K. Schmidmayer, T. Colonius, A quantitative comparison of phase-averaged models for bubbly, cavitating flows, International Journal of Multiphase Flow 115 (2019) 137–143.

[12] S. H. Bryngelson, T. Colonius, Simulation of humpback whale bubble-net feeding models, The Journal of the Acoustical Society of America 147 (2020) 1126–1135.

[13] A. C. Eringen, Nonlinear theory of continuous media, McGraw-Hill, 1962.

[14] M. Rodriguez, E. Johnsen, A high-order accurate five-equations compressible multiphase approach for viscoelastic fluids and solids with relaxation and elasticity, Journal of Computational Physics 379 (2019) 70–90.

[15] G. Altmeyer, E. Rouhaud, B. Panicaud, A. Roos, R. Kerner, M. Wang, Viscoelastic models with consistent hypoelasticity for fluids undergoing finite deformations, Mechanics of Time-Dependent Materials 19 (2015) 375–395.

[16] A. K. Kapila, R. Menikoff, J. B. Bdzil, S. F. Son, D. S. Stewart, Two-phase modeling of deflagration-to-detonation transition in granular materials: Reduced equations, Physics of Fluids 13 (2001) 3002–3024.

[17] S. Gavrilyuk, N. Favrie, R. Saurel, Modelling wave dynamics of compressible elastic materials, Journal of Computational Physics 227 (2008) 2941–2969.

[18] D. Komatitsch, C. Barnes, J. Tromp, Wave propagation near a fluid-solid interface: A spectral-element approach, GEOPHYSICS 65 (2000) 623–631.